Chapman & Hall/CRC Mathematical and Computational Biology Series

Multiscale Cancer Modeling

Edited by
Thomas S. Deisboeck • Georgios S. Stamatakos

CRC Press
Taylor & Francis Group
Boca Raton London New York

CRC Press is an imprint of the
Taylor & Francis Group an **informa** business
A CHAPMAN & HALL BOOK

CHAPTER 6

Multiscale Modeling of Colonic Crypts and Early Colorectal Cancer

Alexander G. Fletcher, Gary R. Mirams, Philip J. Murray, Alex Walter, Jun-Won Kang, Kwang-Hyun Cho, Philip K. Maini, and Helen M. Byrne

CONTENTS

INTRODUCTION

Colorectal cancer accounts for 13% of all cancers in the United Kingdom, with around 35,300 new diagnoses and 16,000 deaths occurring each year (http://info.cancerresearchuk.org). Colorectal cancer is predominantly a disease associated with old age, with 80% of diagnoses being made in patients over the age of 60. As a result of longer life expectancy and declining fertility rates, the proportion of people in this age group is growing faster than any other. In the future, colorectal cancer is therefore sure to rise in prevalence (http://www.who.int/topics/ageing/en).

Colorectal cancers originate from the epithelium that covers the luminal surface of the intestinal tract. This epithelium renews itself more rapidly than any other tissue, being completely replaced every 2–3 days in mice [1] and 5–6 days in humans [2]. The renewal process requires a coordinated program of cell proliferation, migration, and differentiation, which begins in the crypts of Lieberkühn that descend from the epithelium into the underlying connective tissue (see Figure 6.1). At the base of each crypt, a small number of stem cells proliferate continuously, producing transit amplifying cells, which migrate up the crypt axis and divide several times before differentiating into the various cell types that constitute the epithelium (enterocytes, goblet cells, and enteroendocrine cells). Upon reaching the crypt orifice, cells undergo apoptosis and are shed into the lumen.

Under normal conditions, the foregoing cellular processes are tightly regulated by biochemical and biomechanical signals. It is believed that

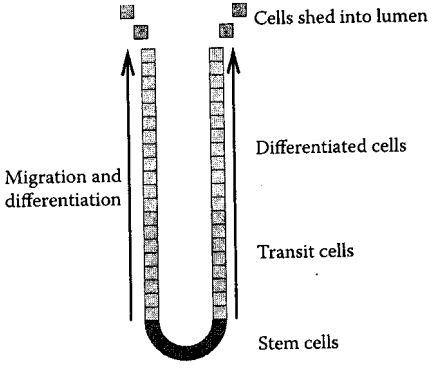

FIGURE 6.1 Schematic of a colonic crypt. Stem cells at the crypt base proliferate continuously, producing transit amplifying cells that migrate up the crypt and differentiate. Cells at the top of the crypt undergo apoptosis and are shed into the lumen.

the first stage of colorectal cancer is caused by the accumulation of genetic alterations that disrupt normal crypt dynamics and cause cells to increase their net proliferation rates. The associated proliferative excess generates biomechanical stress within the crypt, which may deform in order to accommodate the additional cells. The dysplastic cell population may expand further by invading neighboring crypts and/or inducing crypt fission, leading to the formation of an adenoma. Identifying the mechanisms that govern the cellular dynamics of normal crypts is therefore fundamental to understanding the origins of colorectal cancer.

The Wnt pathway is known to play a key role in stem cell maintenance [3,4], cell–cell adhesion [5], cell-fate specification (cell differentiation) [6], central nervous system patterning [7], and tissue development [8,9]. Wnt is an extracellular factor that, when detected by receptors on the outer cell membrane, triggers a cascade of events, culminating in upregulation of intracellular β-catenin levels [10]. A cell's response to Wnt signaling is believed to be mediated predominantly through the concentration and subcellular localization of β-catenin [11]. At the base of the crypt, high levels of Wnt are believed to encourage "stemness" (lack of differentiation), proliferation, and high cell–cell adhesion. By contrast, the low-Wnt environment at the top of the crypt stimulates cells to stop proliferating, differentiate, and weaken their bonds of cell–cell adhesion, preparing them for apoptosis and sloughing into the lumen at the top of the crypt [12].

Most cancers can be initiated by a wide number of different mutations, but almost all colorectal cancers carry activating mutations in a single pathway, the Wnt pathway, with over 80% carrying a double truncation mutation in the gene that encodes the protein APC [13,14]. Thus, the Wnt pathway plays a crucial role in the initiation of colorectal cancer.

As in many cases in biology, colorectal cancer emerges from the interaction of processes that span many different spatial scales. At the genetic level, mutations occur that cause intracellular processes to respond inappropriately to homeostatic cues. This, in turn, affects behavior at the tissue level due to abnormal apoptotic and mitotic responses. Multiscale mathematical modeling can provide insight into how such a complex, highly regulated system operates, both normally and pathologically. A multiscale model cannot account for everything, and in order for a model to be computationally tractable, we must simplify processes at each level. For example, we can exploit different timescales, or use Boolean approaches to simplify the biochemical/metabolic pathways that operate within individual cells. At the tissue level, we need to consider different ways of

modeling a collection of cells, ranging from individual cell-based models right through to the continuum limit. When constructing a multiscale model, which simplifications are appropriate and how processes at each level should be combined remain open questions.

In this chapter, we illustrate the challenges inherent in multiscale modeling by taking colorectal cancer as an example. In the next section, we describe a multiscale model that incorporates simple subcellular models of the Wnt signaling pathway and the cell cycle into a discrete, mechanical model of cell movement in a colonic crypt. This model has been used to investigate several aspects of crypt behavior and to explore different ways of coupling these effects within a fully integrated tissue-level model. The results of these investigations are discussed in the following section. We then conclude with a discussion of alternative modeling approaches and avenues for further work.

STRUCTURE OF THE MULTISCALE MODEL

Mathematical modeling of Wnt regulation of cell activity within intestinal crypts presents a formidable challenge as the Wnt pathway plays an important role in determining a range of cell-level behaviors (e.g., adhesion, proliferation, cell–cell interaction) via mechanisms that are not yet fully understood. In order to investigate how mutations in the Wnt pathway affect crypt dynamics, we therefore require a multiscale framework that takes into account these cell-level behaviors. We now describe a multiscale model in which simple subcellular models of the Wnt signaling pathway and the cell cycle are embedded within a discrete, mechanical model of cell movement.

Wnt Signaling Model

Various mathematical models of Wnt signaling have been proposed. Lee et al. (2003) [15] model the Wnt pathway by a system of nonlinear ordinary differential equations (ODEs), which describe the evolution through time of key cytoplasmic protein concentrations, including β-catenin. This model is analyzed by Mirams et al. (2009) [16], who exploit the different timescales involved to reduce the system to a single ODE, which determines how β-catenin evolves in response to a Wnt stimulus. In addition to providing biological insight into the roles of different proteins on different timescales, this type of systematic model reduction is extremely useful in order to achieve tractable computation times for multiscale simulations.

The localization of subcellular β-catenin has been modeled, also as a system of nonlinear ODEs in [17]. This model is used to examine various hypotheses about underlying biochemical mechanisms; for example, whether β-catenin undergoes a conformational change that favors its involvement in cell–cell adhesion rather than transcription, or whether its fate is determined solely by competition for binding partners.

Wnt-Dependent Cell-Cycle Model

The cell cycle is the orderly sequence of events in which a cell duplicates its contents before dividing into two cells. Since cancer is a disease associated with uncontrolled cell proliferation, the cell cycle constitutes a major target for anti-cancer drug development. This has stimulated extensive experimental research and the formulation of detailed mathematical models designed to enhance understanding of the regulatory networks involved and to explore potential therapeutic interventions. Such models are typically formulated as systems of coupled nonlinear ODEs that characterize changes in the levels of key cell-cycle proteins [18].

We employ the model for the Wnt pathway developed by van Leeuwen et al. (2007) [17] to calculate the associated position-dependent levels of gene expression and use these to link the outcome of the Wnt model to the cell-cycle model developed by Swat et al. (2004) [18], as shown in Figure 6.2. As a result, near the bottom of the crypt, where cells are exposed to high levels of Wnt, the production of Wnt-dependent cell-cycle control proteins is enhanced and cells progress through the cell cycle. In contrast, near the crypt orifice where Wnt levels are low, little or no cell division takes place. Full details of the subcellular models of Wnt signaling and the cell cycle are given in [19].

Mechanical Model

A variety of discrete model frameworks can be used to describe the mechanical behavior of tissue, ranging from lattice-based models, cell-center ("point mass") models, and vertex-based ("non-point-mass") models [20]. We use a tessellation-based, cell-center approach, in which the centers of adjacent cells are connected by linear springs [21] and a Delaunay triangulation is performed at each time step, in order to determine cell–cell connectivity.

Following [21], we determine cell movement by balancing the forces exerted on an individual cell by its neighbors with a drag force.

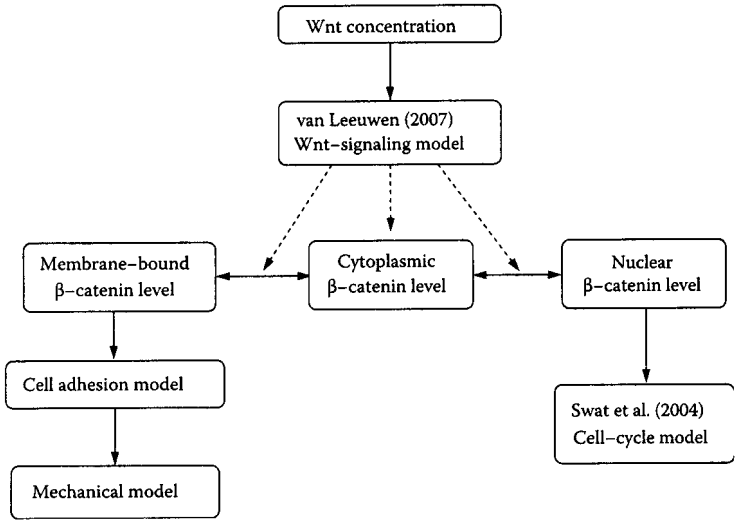

FIGURE 6.2 Influences of the Wnt-signaling model inside a single cell. Note that the Wnt concentration that is experienced depends on the position of the cell within the crypt. The cell-adhesion model influences the motion of the cell, and the cell-cycle model influences the proliferation (and hence again the dynamics) of the cell; thus, the output influences the cell position and changes the input to the Wnt-signaling model. Each cell in a multiscale simulation carries its own Wnt-signaling model.

Specifically, let $\mathbf{r}_i$ be the position of the center of cell i, and define $\mathbf{r}_{ij} = \mathbf{r}_j - \mathbf{r}_i$, and $\hat{\mathbf{r}}_{ij} = \mathbf{r}_{ij}/|\mathbf{r}_{ij}|$. The force exerted on cell i by an adjacent cell j is defined to be

$$\mathbf{F}_{ij} = \mu_{ij}\,\hat{\mathbf{r}}_{ij}(|\mathbf{r}_{ij}| - s_{ij}), \tag{6.1}$$

where μ_{ij} is the spring constant and s_{ij} is the prescribed rest length between cells i and j (i.e., the distance between them for which the force of interaction vanishes). In order to investigate the effect of variable cell–cell adhesion, in the section titled, "Variable Cell–Cell and Cell–Matrix Adhesion" we will consider three choices for the spring constant μ_{ij}. In the first case, $\mu_{ij} \equiv \mu$ takes the same constant value for all neighboring cells i, j. In the second case, to avoid an unrealistically strong attraction between distant neighboring cells, we suppose that μ_{ij} increases with the cell–cell contact length. In this case we take

$$\mu_{ij}(t) = \mu e_{ij}(t)\sqrt{3}/L \tag{6.2}$$

where $e_{ij}(t)$ is the length of the edge between cells i, j and L is the distance between neighboring cell centers in an equilibrium, hexagonal lattice (in such a regular lattice, $e_{ij} \equiv L/\sqrt{3}$, so the first case is recovered). In the third case, we assume that the spring constant depends on the concentration of β-catenin–E-cadherin complexes on the cell membrane, these being determined from the Wnt signaling model (see section titled "Wnt Signaling Model"). In particular following [17], we use the following expression to determine the spring constant connecting cells i and j:

$$\mu_{ij}(t) = \mu e_{ij}(t)\min\left\{B_i(t)C_{Ai}(t)/E_i(t), B_j(t)C_{Aj}(t)/E_j(t)\right\}/Q_A. \tag{6.3}$$

Here, C_{Ai} denotes the Wnt-dependent concentration of adhesion complexes on the surface of cell i; E_i and B_i denote its perimeter and surface area, respectively; and Q_A is a scaling factor that ensures that under equilibrium conditions, the first case is recovered (for details see [19]).

The total force exerted on cell i by its neighboring cells is

$$\mathbf{F}_i = \sum_j \mathbf{F}_{ij}, \tag{6.4}$$

where the sum is over all cells j that are connected to cell i. An overdamped limit is assumed, for which inertial effects are negligible compared to dissipative terms, so that the equation of motion of cell i is

$$\nu_i \frac{d\mathbf{r}_i}{dt} = \mathbf{F}_i, \tag{6.5}$$

where ν_i is the drag coefficient of cell i. In order to investigate the effect of variable cell–substrate adhesion, in the section titled "Variable Cell–Cell and Cell–Matrix Adhesion" we will consider two different cases for the drag coefficient. In the first case, $\nu_i \equiv \nu$ takes the same constant value for all cells i. In the second case, we suppose that the drag coefficient

is proportional to the surface area of contact between a cell and the underlying basement membrane, since a larger cell has more focal adhesions. In this case, we prescribe

$$\nu_i(t) = (d_0 + d_1 B_i(t))\nu, \tag{6.6}$$

where the parameters d_0, d_1 satisfy $d_1 = 2(1-d_0)/(\sqrt{3}L^2)$ so that for an equilibrium, hexagonal lattice we recover the first case.

The equation of motion is discretized numerically using a forward Euler approach, from which it is straightforward to deduce that the position of the cell at time $t + \Delta t$ is related to its position at time t via

$$\mathbf{r}_i(t+\Delta t) = \mathbf{r}_i(t) + \frac{\Delta t}{\nu_i}\mathbf{F}_i(t). \tag{6.7}$$

The rest length s_{ij} between cells is assumed to be the typical diameter of a crypt cell. When a cell divides, as determined by its internal cell-cycle model, a new cell is placed at a smaller fixed distance in a random direction. The rest length s_{ij} between the two daughter cells increases linearly over the course of an hour to the mature cell rest length (to emulate the mitosis phase of the cell cycle). Thus, the nuclear β-catenin influences the cell-cycle model (and so indirectly the mechanics as extra cells are added), and membrane-bound β-catenin influences the mechanical model. Intracellular β-catenin is influenced by cell position due to the imposed Wnt gradient along the crypt axis, which feeds back and influences the cell cycle and mechanical models.

Methodology and Implementation Using Chaste

For simplicity we focus on an individual crypt, treating the three-dimensional tubular crypt as a monolayer of cells lying on a cylindrical surface. We take a discrete approach, modeling each cell individually. For simulation purposes, it is convenient to roll the crypt out onto a flat planar domain and impose periodic boundary conditions on the left and right sides. The structure of the multiscale model is depicted in Figure 6.3. It comprises the three interlinked modules discussed earlier: a model of the Wnt signaling pathway [17]; a model of the cell cycle [18], which together with the Wnt model determines each cell's proliferative behavior; and a mechanical model of cell movement [21].

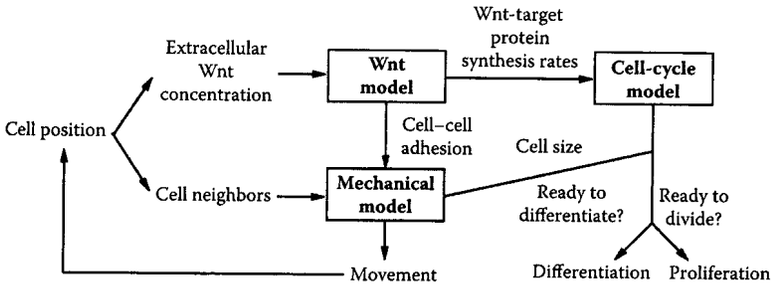

FIGURE 6.3 Diagram illustrating the modular nature of our multiscale crypt model. The occurrence of cellular events (proliferation, differentiation, migration) is monitored at discrete time steps t_n. By coupling Wnt signaling, cell cycle, and mechanical models, we are able to predict the spatiotemporal behavior of every cell at time t_{n+1}, given the state of the system (e.g., intracellular protein levels, cell position, Wnt stimulus, location of neighboring cells) at time t_n and the model parameters.

Chaste (Cancer, Heart and Soft Tissue Environment) is a collaborative software development project that is designed to act as a high-quality multi purpose library supporting computational simulations for a wide range of biological problems. In this context, "high-quality" means that the software is extensible, robust, fast, accurate, and maintainable and uses state-of-the-art numerical techniques. It is also open-source, and so can be adapted by other developers. Chaste has been developed by a multidisciplinary team including mathematicians and software engineers. This ensures that the code is well structured as a piece of software, while at the same time practical and useful as a computational modeling tool. While it is a generic extensible library, to date attention has focused on the fields of cardiac electrophysiology and tumor growth [22].

Chaste is written using an agile method adapted from a technique known as "eXtreme Programming" [23]. This programming methodology is characterized by test-driven development, in which a test is written to cover any new functionality in the code before it is implemented [24]. This enables developers rapidly to discover, diagnose, and fix bugs in the code. The main Chaste code has been written in object-oriented C++, which leads naturally to more modular code: software that is easier to abstract, to modify, and to document. This is especially advantageous for multiscale models of the type considered in this chapter, as it allows different simulations to be generated in a straightforward manner, by using the

appropriate components, and preventing unnecessary repetition of code. Further details on Chaste, including visualization movies and user support, are available at http://web.comlab.ox.ac.uk/chaste/.

RESULTS

The multiscale model described earlier has been used to study several aspects of normal crypt behavior and to investigate coupling of processes occurring across a number of spatial scales. We now summarize our results to date.

Wnt Signaling in the Crypt

It has been postulated that a Wnt gradient exists in the crypt, stimulating proliferation at the base and promoting differentiation toward the top. Use of the multiscale model in [19] led us to predict that a Wnt gradient along the entire crypt axis is not necessary to provide a β-catenin (and hence proliferation) gradient. Indeed, Wnt expression in a neighborhood of (approximately) the three cells at the base of the crypt is sufficient to establish a proliferation pattern that extends throughout the crypt; this is because cells move up the crypt more quickly than their Wnt signaling pathways can adapt to the reduction in the local Wnt stimulus. These results are illustrated in Figure 6.4, where the height at which a cell divides, and the corresponding cell-cycle duration are recorded in a scatter graph, for a crypt containing stationary cells and another containing cells that move.

Van Leeuwen et al. (2009) [19] perform simulations of the multiscale model in order to compare the distribution of β-catenin inside each cell in the crypt, under the two hypotheses stated earlier (the simpler hypothesis states that β-catenin fate is determined by competition for binding partners, whereas the second hypothesis proposes that β-catenin can undergo a conformational change that favors binding to E-cadherin at the cell membrane). The results of such simulations are shown in Figure 6.5. The different patterns of β-catenin associated with each hypothesis suggest that it should be possible to discriminate between them by measuring the distribution of β-catenin within the epithelial cells that line a crypt.

Mitotic Labeling

Mitotic labeling experiments are often used to characterize the proliferation and cellular dynamics of intestinal crypts (e.g., [25]). These

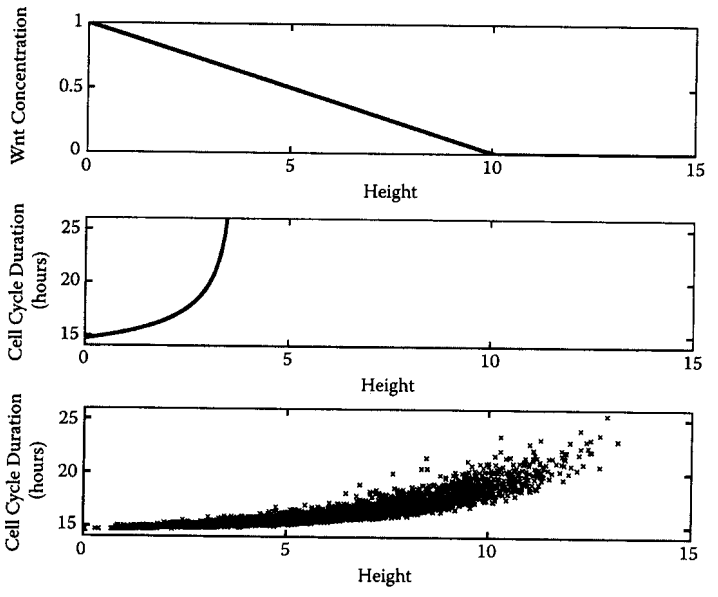

FIGURE 6.4 The cell-cycle duration response of a coupled Wnt signaling and cell-cycle model to varying Wnt stimuli. Simulation performed in a crypt that is 23 cells high. Top: The Wnt gradient imposed upon the crypt. Middle: Cell-cycle durations if cells are held in fixed positions; the predicted Wnt threshold for cell division is about 0.66. Bottom: Cell-cycle durations in a dynamic crypt simulation; for each cell in the simulation, the cell-cycle time is plotted as a function of the cell's position at the time of division.

experiments involve injecting laboratory rodents with an agent that is incorporated into cells during the S phase of the cell cycle and is passed on to their progeny. The distribution of clonal populations can be monitored over time by dissecting the crypts longitudinally and recording the positions of labeled cells along the two dissection lines. Given a sample containing several crypts, the outcome of the experiment is summarized in the form of a labeling-index (LI) curve, which shows the percentage of labeled cells per cell position at the time of sacrifice. We have used our multiscale model to perform similar in silico LI experiments. At time $t = 0$, we label all cells that are in the S phase. The simulation proceeds under the assumption that labeled cells behave in the same manner as their unlabeled counterparts, except that they transmit labels to their daughters. After a fixed time, we stop the simulation and perform a virtual crypt dissection. The LI curves obtained from the virtual dissections descend

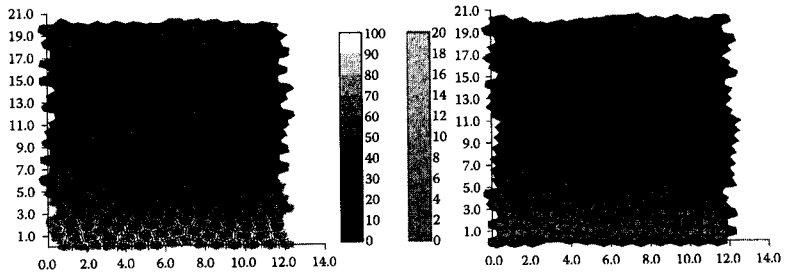

FIGURE 6.5 **(See color insert following page 40)** A quasi-steady simulation of cells stained for β-catenin, under two different hypotheses, as discussed [17] and as implemented in van Leeuwen et al. (2009). The Chaste visualizer displays the concentrations of nuclear and cytoplasmic levels of β-catenin on the green scale and membrane-bound β-catenin on the grey scale, facilitating a qualitative comparison with crypt staining or GFP-labeling experiments.

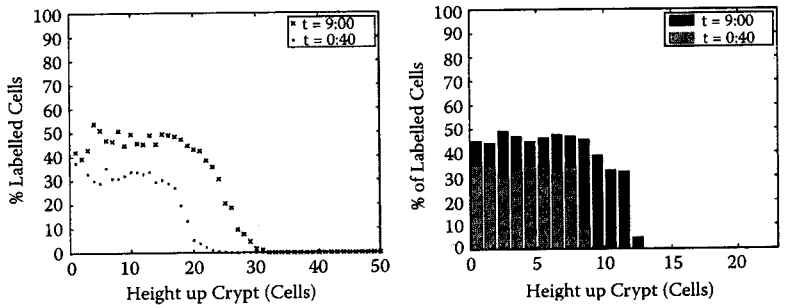

FIGURE 6.6 Results of virtual labeling-index experiments. Data obtained from 250 crypt simulations. Height up the crypt is expressed in units of length L. (left) Percentage of labeled cells per position along the dissection lines. Bullet points and crosses correspond to results obtained 40 min and 9 h after labeling, respectively. (right) True average percentage of labeled cells as a function of distance from the crypt base. Grey and black bars represent the results obtained 40 min and 9 h after labeling, respectively. (Reproduced with permission from van Leeuwen et al. *Cell Prolif.* 42 doi:10.1111/j.1365–2184.2009.00627.x. 2009.)

gradually, suggesting a smooth decrease in the percentage of labeled cells with increasing distance from the crypt base (Figure 6.6a). However, our model shows clearly segregated proliferative and differentiated populations, with an abrupt boundary between labeled and unlabeled cells in the averaged data (Figure 6.6b). This discrepancy is due to dissection and

suggests that data from standard LI experiments may tend to overestimate the true position of the labeled cells.

Clonal Expansion and Niche Succession

Over time, the progeny of a single stem cell may dominate an entire crypt via a process termed *monoclonal conversion*, since the resulting crypt consists of a single clonal population [26]. Since mutations occur in single cells, the process of monoclonal conversion is important in the context of carcinogenesis as a mutant clone descended from this single cell has to persist in a crypt, by proliferating and eventually dominating it, in order for a mutant clone to gain a foothold in the colonic epithelium. Once a crypt has become mutant monoclonal, the mutant population can spread to neighboring crypts, either by top-down invasion, or through a process called *crypt fission* whereby a crypt divides into two.

Our multiscale model is ideally suited to study expansion of a clonal population *in silico*, and to predict conditions under which a crypt may become monoclonal. The main advantage is the ability to follow a clone's progress in real time, something that is impossible with current experimental techniques. We simulate the experiments of Taylor et al. (2003) [27], in which the progeny of cells with mitochondrial DNA (mtDNA) mutations that are functionally neutral are tracked. Such cells express a phenotype, for example, cytochrome-c oxidase (CcO) deficiency, which appear blue in histochemical stainings. In addition to wild-type crypts, Taylor et al. (2003) [27] observed crypts either partially or wholly filled with blue cells. In the former, "there is a ribbon of CcO-deficient cells within an otherwise normal crypt that is entirely compatible with the view that there are multiple stem cells in some crypts."

We investigated clonal expansion for two alternative model assumptions: first, following [21], the stem cells were fixed at the crypt base and assumed to divide asymmetrically; and second, following [19], the stem cells were unpinned and their proliferative behavior determined by the local Wnt stimulus. The results presented in columns I and II of Figure 6.7 reveal that if the stem cells are fixed in position, then an initial blue-stained stem cell invariably generates a thin, blue trail that moves upward toward the crypt orifice. Discontinuities in the clone can occur, due to waiting times between consecutive cell divisions. Importantly, although the trail's pattern can change in time, it does not expand laterally. Thus, under the original model assumptions, we are unable to capture the broad, wavy blue ribbons observed by Taylor et al. (2003) [27]. In contrast, as columns III and IV of Figure 6.7 show,

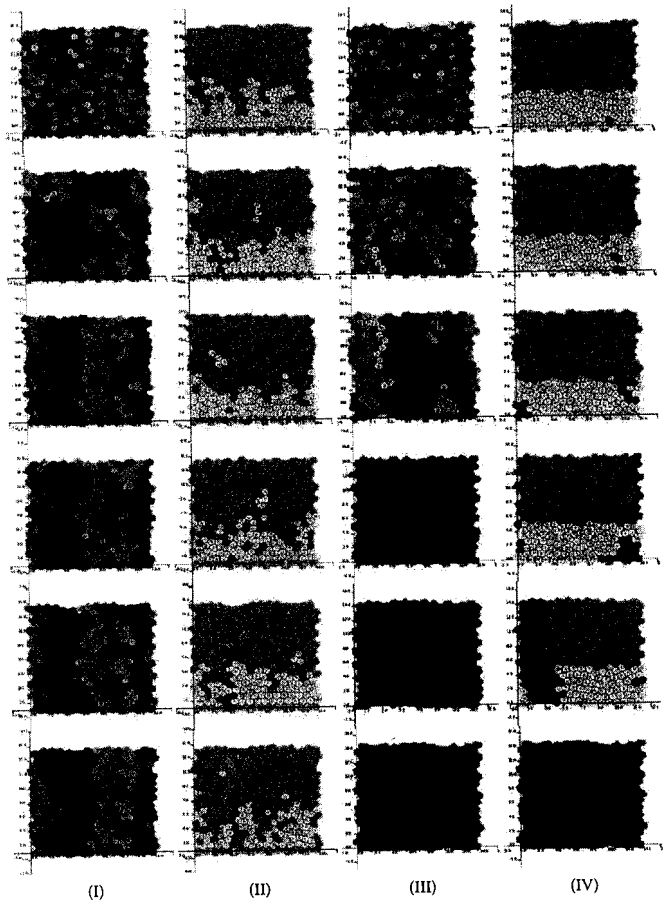

FIGURE 6.7 **(See color insert following page 40)** Clonal expansion in the crypt. Each column shows six snapshots from two independent *in silico* experiments performed with the model in [21] (columns I and II) and standard ($\mu_{ij} \equiv \mu$ and $\nu_i \equiv \nu$) model in [19] (columns III and VI), respectively. At time $t = 0$, a single cell is stained with a blue dye. This label is transmitted from generation to generation, giving rise to a clonal population of labeled cells. Columns II and IV highlight how the labeled populations evolve in time, whereas columns I and II show the clonal composition of the crypt. In column II, the stem cells, which are pinned to the base of the crypt, are highlighted in green. In the DMC simulation (columns III and IV), the population of labeled cells eventually takes over the crypt. (Reproduced with permission from van Leeuwen et al. *Cell Prolif.* 42 doi:10.1111/j.1365–2184.2009.00627.x. 2009.)

if the stem cells are free to move and cell fate is determined by local environmental conditions then, over time, clonal populations either expand in size or become extinct. In particular, the progeny of a single cell will eventually populate the entire crypt, and further, this cell will always eventually leave the crypt. These results suggest that cell "stem-ness" may depend on local biochemical cues rather than being an intrinsic property of a cell.

Variable Cell–Cell and Cell–Matrix Adhesion

As discussed in the section titled "Mechanical Model," we have considered a number of different cases regarding the dependence of cell–cell and cell–matrix adhesion on cell shape and Wnt signaling. In order to compare the impact of these different model assumptions on cell kinetics, we followed the dynamics of a standard crypt simulation (in which $\mu_{ij} \equiv \mu$ and $\nu_i \equiv \nu$; denoted NN) for 800 h and then repeated this for three other cases: the case of area-dependent cell–matrix adhesion only (denoted YN); the case of contact-edge-dependent cell–cell adhesion only (denoted NY); and the case of both contact-edge-dependent cell–cell adhesion and area-dependent cell–matrix adhesion (denoted YY). Results are shown in Figure 6.8. We find that YN cells located near the crypt base are larger than their NN counterparts. This is because in the YN case, if two cells of different sizes are attached by a compressed spring, the smaller cell moves apart more rapidly than the larger one. Consequently, small newborn cells leave the crypt base quicker than in the NN case. We also find that in the NY case, cells are more hexagonal in shape, and the crypt is densely populated with closely packed cells. In this case, the dependence of spring forces on cell size could eventually lead to a critical situation in which migration ceases completely; this can be prevented in the YY case, where variable cell–matrix and cell–cell adhesion are considered.

Hypotheses for Crypt Invasion

It is a matter of great debate how a single, mutant cell establishes a mutant epithelium within the crypt [28]. Two mechanisms have been suggested: top-down and bottom-up morphogenesis. Under top-down morphogenesis, a mutant cell at the top of a crypt expands not only laterally and downward but also invades (adjacent) crypts containing normal epithelium [29]. Under bottom-up morphogenesis, the mutant cell originates at the base of the crypt and increases in number through proliferation, until its progeny populate the entire crypt [30].

The model has been used to investigate the behavior of cells with APC or β-catenin mutations, the most common in colorectal cancer [31], within

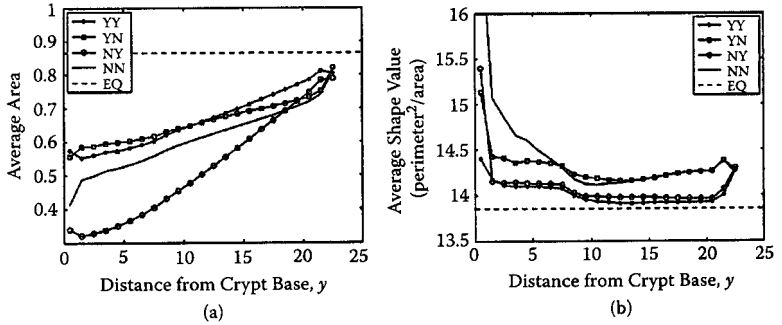

FIGURE 6.8 Dependence of cell size and geometry on cell adhesion. Results from four crypt simulations in dynamic equilibrium with different mechanical assumptions: NN = standard model; YN = area-dependent cell-matrix adhesion only; NY = contact-edge-dependent cell–cell adhesion only; YY = contact-edge-dependent cell–cell adhesion and cell-size-dependent cell–matrix adhesion; and EQ = values for hexagonal equilibrium lattice. Height up the crypt is expressed in units of length L. (a) Average cell area as a function of cell position. (b) Average shape value (perimeter^2/area) as a function of cell position. (Reproduced with permission from van Leeuwen et al. *Cell Prolif.* 42 doi:10.1111/j.1365–2184.2009.00627.x. 2009.)

the crypt. Mutations in these proteins enable cells to proliferate independently of Wnt [10]. Such mutant cells have also been shown to have a more rigid cytoskeleton [32], higher levels of cell–stroma [13] and stronger cell–cell adhesion [33]. We model these changes by allowing the damping constant to depend on whether the cell is mutant or not. The model was then used to establish the properties a mutant cell would require to allow top-down and bottom-up morphogenesis to occur. Numerical simulations reveal that mutant cells, which do not proliferate in a Wnt-dependent manner, can establish themselves within the crypt if they have higher levels of cell–substrate adhesion and a more rigid cytoskeleton. Top-down morphogenesis requires higher levels of cell–substrate adhesion and cytoskeleton rigidity than bottom-up morphogenesis.

DISCUSSION

In this chapter, we have presented a computational framework that allows us to integrate biological processes that act across a broad range of spatial scales. We have considered the model in the context of colorectal cancer and used it to address issues such as the role of Wnt signaling in the crypt,

the process of monoclonal conversion, and the effects of model assumptions regarding cell–cell and cell–stroma adhesion.

In modeling the dependence of cell proliferation on Wnt signaling, we have neglected other pathways that are known to play an important role in regulating crypt structure.

Bone morphogenetic protein (BMP) signaling, which converges with the Wnt pathway to regulate β-catenin, is thought to control the process of stem cell self-renewal [34]. Dysregulation of BMP signaling can result in crypt fission and excessive quantities of crypt-like structures [35], as observed in humans with juvenile polyposis syndrome. The control of the Eph/ephrin signaling pathway may also be highly relevant in ensuring the proper crypt structure, as demonstrated by the fact that loss of expression of EphB receptors is correlated with the onset of invasive behavior [36]. Lastly, all proliferating cells in the crypt largely depend not only on Wnt but also Notch signaling; neither pathway is sufficient on its own to maintain proliferation [37]. Future work will involve the construction of mathematical models to investigate how these different pathways interact to control the proliferation of cells within the crypt, and incorporation of these models within the multiscale framework described in this chapter.

Many of the results presented in the section titled "Results" are consistent with independent experimental observations of colonic crypts. However, to have confidence in the model, we should account for the model assumptions that are implicit in our cell-center model by contrasting our model with other discrete model frameworks. In particular, it remains to be established which discrete model is best suited to a given biological problem.

Cell-center models, such as that presented in the section titled "Mechanical Model," can efficiently simulate cell proliferation, growth, and migration in the crypt. Moreover, it is straightforward to incorporate differential cell–cell adhesion [38–41] and to vary cell–substrate adhesion by varying the cellular drag coefficients. However, a disadvantage of such cell-center models is their reliance on the Delaunay triangulation, meaning that the number of vertices and the shapes of the cells do not change smoothly [42]. An alternative approach is cell-vertex modeling, in which cells are treated as polygons in 2D or polyhedra in 3D [43]. In cell-vertex models, the dynamics of each cell is governed by the movement of its vertices, these being determined by explicitly calculating the resultant forces or minimizing a global energy function. Cell-vertex models can describe changes in cell shape more realistically than cell-center models.

This is particularly important in the context of crypt modeling as we may wish to couple cell shape and surface areas to subcellular control models, as described in the section titled "Mechanical Model." Cell-vertex models are particularly suitable for modeling differential cell–cell adhesion, an important feature of cell dynamics in the crypt, as common mutations in colorectal epithelial cells are thought to affect cell–cell adhesion. However, the inclusion of differential cell–substrate adhesion is not so straightforward, as the drag terms include contributions from cells surrounding a given vertex. While cell-vertex models do not require the computation of a Delaunay triangulation at each time step, the higher spatial resolution considered in cell-vertex models results in a larger system dimension than that of a cell-center model. Osborne et al. (2010) [44] have developed a cell-vertex model of the crypt and, using numerical simulations, have found that it exhibits qualitatively similar behavior to our cell-center model.

A major problem with discrete models, especially those incorporating stochastic behavior, is their computational intensity. For example, in the case of our multiscale model, a large number of simulations are needed to determine how a proliferative advantage bestowed on mutant cells translates into an increase in their probability of becoming the dominant clonal population within a crypt, and how this increased probability varies with the location of the initial mutation within the crypt. Moreover, as the molecular details of subcellular pathways become increasingly more complex, systematic and rational model reduction becomes a critically important tool, as a modeling approach that simply includes all known molecular details quickly becomes intractable. One resolution of this problem is to develop a continuum model that replicates the qualitative features of the original discrete model. We can then apply mathematical techniques to analyze the coarse-grained model and, for instance, establish quickly the necessary phenotypic traits for mutant cells to take over a crypt via the top-down and/or bottom-up morphogenesis. Such continuum models can be derived either formally [45] or phenomenologically [44].

By viewing the epithelial cells that line a crypt as a one-dimensional chain of connected linear springs, Murray et al. (2009) [45] have formally derived a continuum model for cell number density. This model comprises a reaction-diffusion equation with a spatially non-uniform proliferation term and a nonlinear diffusive flux term, with diffusion coefficient

$$D(q)=\frac{\mu}{\nu q^2}, \tag{6.8}$$

where q denotes the cell number density and μ and ν denote the spring constant (assumed the same for all cell–cell interactions) and damping constant (assumed the same for all cells). As Figure 6.9 shows, there is generally good qualitative agreement between the cell velocities obtained with this coarse-grained model and those obtained from our 2D multiscale model. A discrepancy between the two models for smaller values of μ arises from the assumption that the crypt is one-dimensional.

Using a phenomenological approach, Osborne et al. (2010) [44] have developed a 2D continuum model for a crypt in which cells are treated as an incompressible viscous fluid obeying Darcy's law. As Figure 6.10 shows, model simulations compare reasonably well with the multiscale model, as well as with a cell-vertex model of the crypt. However, the continuum

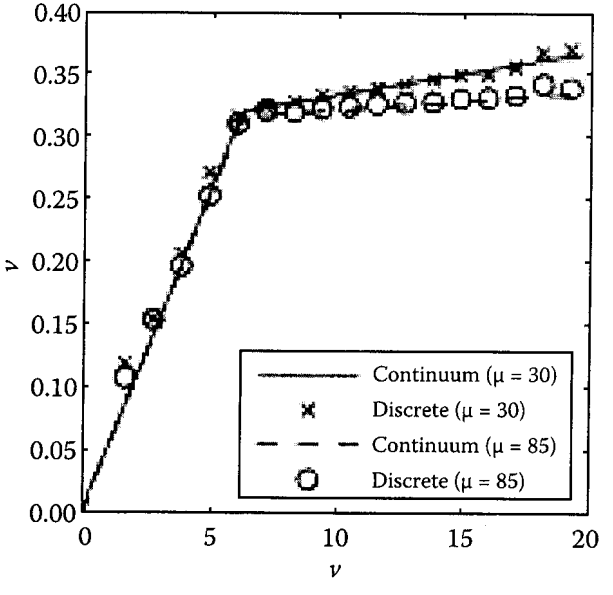

FIGURE 6.9 Steady-state crypt velocities, v, plotted against crypt height, y. Thousand simulations of a 2D periodic crypt were run, and the average cell velocities (markers) were compared with the velocities predicted by the corresponding continuum model (lines). In this plot $y_C = 0.3$, $T_C = 14$, and $L = 20.1$. The circles and solid line correspond to $\mu = 40$, whereas the crosses and dashed line correspond to $\mu = 80$.

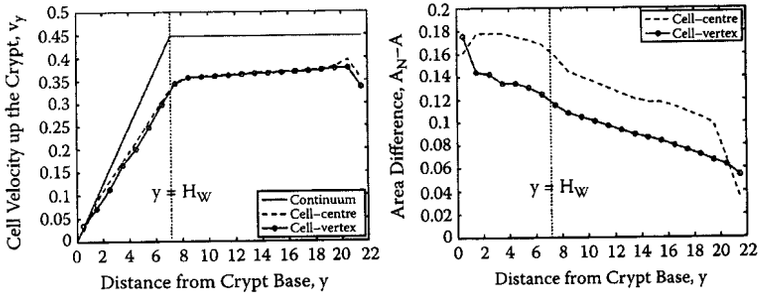

FIGURE 6.10 Comparison of cell-center, cell-vertex, and continuum crypt models. In each graph, the dotted vertical line $y = H_W$ delineates the upper boundary of the Wnt-stimulated region: cells proliferate for $y \leq H_W$, and for $y > H_W$ they do not. Left: Dependence of average speed up the crypt axis on distance from the crypt base. Right: Dependence of average cell compression (natural cell area minus actual cell area) on distance from the crypt base.

model does slightly overestimate cell velocities within the crypt, as a result of the assumption of cell incompressibility, which in 1D corresponds to the limit $\mu \to \infty$ in the Murray et al. model [45].

There are now a multitude of such integrative models in the literature (see, for example [46–48]). Similar to these, the modeling approach discussed in this chapter suffers from the problem that we have made simplifications at each scale and, while we can investigate the errors induced at each level, we have not developed a theory for how to do this across scales. This remains an open question. Therefore, an important future challenge for the modeling community is to develop a systematic way of constructing such models. As described earlier, one possible way to approach this might be in the recent research that aims to develop continuum models of individual-based computational schemes (see, for example, [45,49,50]). This allows us not only to see precisely where the different modeling assumptions at the cell-level affect tissue-level behavior, but may also allow us to, in the future, use the well-developed mathematical machinery for partial differential equations to address key problems in multiscale modeling.

ACKNOWLEDGMENTS

The authors gratefully acknowledge funding from the EPRSC as part of the Integrative Biology program (GR/572023/01). PJM and PKM were partially supported by NIH Grant U56CA113004 from the National Cancer Institute. PJM, KHC, PKM, and HMB were partially supported by PMI2 (British Council). PKM was partially supported by a Royal Society Wolfson Merit Award. JWK and KHC acknowledge the support received from the National Research Foundation of Korea grant funded by the Korea Ministry of Education, Science & Technology, through the Systems Biology grant (20090065567), the Nuclear Research grant (M20708000001-07B0800-00110), the 21C Frontier Microbial Genomics and Application Center Program (Grant 11-2008-10-004-00), the World Class University grant (R32-2008-000-10218-0), and the BRL (Basic Research Laboratory) grant (2009-0086964).

REFERENCES

1. Okamoto, R. and Watanabe, M. 2004. Molecular and clinical basis for the regeneration of human gastrointestinal epithelia. *J. Gastroenterol.* 39:1–6.
2. Ross, M.H., Kaye, G.I., and Pawlina W. 2003. *Histology: A Text and Atlas.* Lippincott Williams & Wilkins.
3. Reya, T. and Clevers, H. 2005. Wnt signalling in stem cells and cancer. *Nature* 434:843–850.
4. Pinto, D. and Clevers, H. 2005. Wnt control of stem cells and differentiation in the intestinal epithelium. *Exp. Cell Res.* 306:357–363.
5. Hinck, L., Nelson, W.J., and Papkoff, J. 1994. Wnt-1 modulates cell-cell adhesion in mammalian cells by stabilizing β-catenin binding to the cell adhesion protein cadherin. *J. Cell Biol.* 124:729–741.
6. Logan, C.Y. and Nusse, R. 2004. The Wnt signaling pathway in development and disease. *Annu. Rev. Cell Dev. Biol.* 20:781–810.
7. Hall, A.C., Lucas, F.R., and Salinas, P.C. 2000. Axonal remodeling and synaptic differentiation in the cerebellum is regulated by WNT-7a signaling. *Cell* 100:525–535.
8. Church, V.L. and Francis-West, P. 2002. Wnt signalling during limb development. *Int. J. Dev. Biol.* 46:927–936.
9. Nelson, W.J. and Nusse, R. 2004. Convergence of Wnt, β-catenin, and cadherin pathways. *Science* 303:1483–1487.
10. Ilyas, M. 2005. Wnt signalling and the mechanistic basis of tumour development. *J. Pathol.* 205:130–144.
11. Fodde, R. and Brabletz, T. 2007. Wnt/β-catenin signaling in cancer stemness and malignant behavior. *Curr. Opin. Cell Biol.* 19:150–158.
12. Gaspar, C. and Fodde, R. 2004. Wnt signalling/APC dosage effects in tumorigenesis and stem cell differentiation. *Int. J. Dev. Biol.* 48:377–386.
13. Sansom, O.J., Reed, K.R., Hayes, A.J. et al. 2004. Loss of Apc in vivo immediately perturbs Wnt signaling, differentiation, and migration. *Genes Dev.* 18:1385–1390.
14. Sansom, O.J., Meniel, V.S., Muncan, V. et al. 2007. Myc deletion rescues Apc deficiency in the small intestine. *Nature* 446:676–679.

15. Lee, E., Salic, A., Kruger, R., Heinrich, R., and Kirschner, M.W. 2003. The roles of APC and Axin derived from experimental and theoretical analysis of the Wnt pathway. *PLoS Biol.* 1:116–132.
16. Mirams, G.R., Byrne, H.M., and King, J.R. 2010. A multiple timescale analysis of a mathematical model of the Wnt/ β-catenin signalling pathway. *J. Math. Biol.* 60, 131–160.
17. van Leeuwen, I.M.M., Byrne, H.M., Jensen, O.E., and King, J.R. 2007. Elucidating the interactions between the adhesive and transcriptional functions of β-catenin in normal and cancerous cells. *J. Theor. Biol.* 247:77–102.
18. Swat, M., Kel, A., Herzel, H. 2004. Bifurcation analysis of the regulatory modules of the mammalian G1/S transition. *Bioinformatics* 20:1506–1511.
19. van Leeuwen, I.M.M., Mirams, G.R., Walter, A. et al. 2009. An integrative computational model for intestinal tissue renewal. *Cell Prolif.* 42 doi:10.1111/j.1365–2184.2009.00627.x.
20. Weliky, M., Minsuk, S., Keller, R., and Oster, G. 1991. Notochord morphogenesis in Xenopus laevis: simulation of cell behavior underlying tissue convergence and extension. *Development* 113:1231–1244.
21. Meineke, F.A., Potten, C.S., and Loeffler, M. 2001. Cell migration and organization in the intestinal crypt using a lattice-free model. *Cell Prolif.* 34:253–266.
22. Pitt-Francis, J., Pathmanathan, P., Bernabeu, M.O. et al. 2009. Chaste: a test-driven approach to software development for biological modelling. *Computer Physics Communications* 180, 2452–2471.
23. Beck, K. and Andres, C. 2004. *Extreme Programming Explained: Embrace Change.* Addison-Wesley, Boston.
24. Pitt-Francis, J., Bernabeu, M.O., Cooper, J. et al. 2008. Chaste: using agile programming techniques to develop computational biology software. *Phil. Trans. Roy. Soc. A* 366:3111–3136.
25. Sunter, J.P., Appleton, D.R., De Rodriguez, M.S.B., Wright, N.A., and Watson, A.J. 1979. A comparison of cell proliferation at different sites within the large bowel of the mouse. *J. Anat.* 129, 833–842.
26. McDonald, S.A.C., Preston, S.L., Greaves, L.C. et al. 2006. Clonal expansion in the human gut: mitochondrial DNA mutations show us the way. *Cell cycle* 5:808–811.
27. Taylor, R.W., Barron, M.J., Borthwick, G.M. et al. 2003. Mitochondrial DNA mutations in human colonic crypt stem cells. *J. Clin. Invest.* 112:1351–1360.
28. Wright, N.A. 2000. Epithelial stem cell repertoire in the gut: clues to the origin of cell lineages, proliferative units and cancer. *Int. J. Exp. Pathol.* 81:117–143.
29. Shih, I.M., Wang, T.L., Traverso, G. et al. 2001. Top-down morphogenesis of colorectal tumors. *Proc. Natl. Acad. Sci. USA* 98:2640–2645.
30. Preston, S.L., Wong, W.M., Chan, A.O. et al. 2003. Bottom-up histogenesis of colorectal adenomas: origin in the monocryptal adenoma and initial

31. Giles, R.H., van Es, J.H., and Clevers, H. 2003. Caught up in a Wnt storm: Wnt signaling in cancer. *Biochim. Biophys. Acta.* 1653:1–24.
32. Näthke, I. 2006. Cytoskeleton out of the cupboard: colon cancer and cytoskeletal changes induced by loss of APC. *Nat. Rev. Cancer* 66:967–974.
33. Bienz, M. 2005. β-catenin: a pivot between cell adhesion and Wnt signalling. *Curr. Biol.* 15:64–67.
34. He, X.C., Zhang, J., Tong, W.-G. et al. 2004. BMP signaling inhibits intestinal stem cell self-renewal through suppression of Wnt-β-catenin signaling. *Nat. Genet.* 36:1117–1121.
35. Haramis, A.P.G., Begthel, H., van den Born, M. et al. 2004. *De novo* crypt formation and juvenile polyposis on BMP inhibition in mouse intestine. *Science* 303:1684–1686.
36. Battle, E., Bacani, J., Begthel, H. et al. 2005. EphB receptor activity suppresses colorectal cancer progression. *Nature* 435:1126–1130.
37. van Es, J.H., van Gijn, M.E., Riccio, O. et al. 2005. Notch/γ-secretase inhibition turns proliferative cells in intestinal crypts and adenomas into goblet cells. *Nature* 435:959–963.
38. Galle, J., Loeffler, M., and Drasdo, D. 2005. Modeling the effect of deregulated proliferation and apoptosis on the growth dynamics of epithelial cell populations in vitro. *Biophys. J.* 88:62–75.
39. Ramis-Conde, I., Drasdo, D., Anderson, A.R.A., and Chaplain, M.A.J. 2008. Modelling the influence of the E-cadherin-β-catenin pathway in cancer cell invasion: a multi-scale approach. *Biophys. J.* 95:155–165.
40. Schaller, G. and Meyer-Hermann, M. 2005. Multicellular tumor spheroid in an off-lattice Voronoi-Delaunay cell model. *Phys. Rev. E* 71:51910.
41. Walker, D.C., Southgate, J., Hill, G. et al. 2004. The epitheliome: agent-based modelling of the social behaviour of cells. *Biosystems* 76:89–100.
42. Brodland, G.W. 2004. Computational modeling of cell sorting, tissue engulfment, and related phenomena: a review. *ASME Applied Mechanics Rev.* 57:1–30.
43. Honda, H., Tanemura, M., and Nagai, T. 2004. A three-dimensional vertex dynamics cell model of space-filling polyhedra simulating cell behavior in a cell aggregate. *J. Theor. Biol.* 226:439–453.
44. Osborne, J.M., Walter, A., Kershaw, S.K. et al. 2010. A hybrid approach to multiscale modeling of cancer. *Phil. Trans. Roy. Soc. A* (in press).
45. Murray, P.J., Edwards, C.E., Tindall, M.J., and Maini, P.K. 2009. From a discrete to a continuum model of cell dynamics in 1D. In preparation.
46. Alarcón, T., Byrne, H.M., and Maini, P.K. 2005. A multiple scale model for tumor growth. *Multiscale Model Simul.* 3:440–475.
47. Ribba, B., Saut, O., Colin, T., Bresch, D., Grenier, E., and Boissel, J.P. 2006. A multiscale mathematical model of avascular tumor growth to investigate the therapeutic benefit of anti-inasive agents. *J. Theor. Biol.* 243:532–541.
48. Macklin, P., McDougall, S., Anderson, A.R.A., Chaplain, M.A.J., Cristini, V., and Lowengrub, J. 2009. Multiscale modelling and nonlinear simulation of

49. Alber, M., Chen, N., Lushnikov, P., and Newman, S. 2007. Continuous macroscopic limit of a discrete stochastic model for interaction of living cells. *Phys. Rev. Lett.* 99:168102.
50. Fozard, J.A., Jensen, O.E., Byrne, H.M., and King, J.R. 2009. Continuum approximations of individual-based models for epithelial monolayers. *Math. Med. Biol.* doi:10.1093/imammb/dqp015.